communications earth & environment

Article

https://doi.org/10.1038/s43247-024-01907-5

Atlantic Meridional Overturning Circulation slowdown modulates wind-driven circulations in a warmer climate

Check for updates

Mohima Sultana Mimi ✉ & Wei Liu

Wind-driven and thermohaline circulations, two major components of global large-scale ocean circulations, are intrinsically related. As part of the thermohaline circulation, the Atlantic Meridional Overturning Circulation has been observed and is expected to decline over the twenty-first century, potentially modulating global wind-driven circulation. Here we perform coupled climate model experiments with either a slow or steady Atlantic overturning under anthropogenic warming to segregate its effect on wind-driven circulation. We find that the weakened Atlantic overturning generates anticyclonic surface wind anomalies over the subpolar North Atlantic to decelerate the gyre circulation there. Fingerprints of overturning slowdown are evident on Atlantic western boundary currents, encompassing a weaker northward Gulf Stream and Guiana Current and a stronger southward Brazil Current. Beyond the Atlantic, the weakened Atlantic overturning causes a poleward displacement of Southern Hemisphere surface westerly winds by changing meridional gradients of atmospheric temperature, leading to poleward shifts of the Antarctic Circumpolar Current and Southern Ocean meridional overturning circulations.

Wind-driven and thermohaline circulations characterize global large-scale ocean circulations. Although both components are typically thought to be driven by separate surface fluxes—the former by surface winds, the latter by surface heat and freshwater fluxes—wind-driven and thermohaline circulations are inextricably linked[1]. The thermohaline circulation, for example, might collapse if surface winds disappeared[2] or considerably weakened[3].

The Atlantic Meridional Overturning Circulation (AMOC), as part of the thermohaline circulation, has been suggested to closely link to the wind-driven subpolar gyre circulation (SPG) in the North Atlantic. Since the 1990s, either the AMOC[4] or the North Atlantic SPG[5] has experienced a declining trend, implying that a weakened AMOC is associated with a decelerated SPG, accompanied by a weakened and southward-shifted Gulf Stream[6–9]. On the other hand, a slowing AMOC is suggested to relate to an intensified North Atlantic SPG[10,11] and a northward displacement in the Gulf Stream path[12]. These contrasting relationships between the AMOC and North Atlantic SPG potentially stem from the arguments that the observed SPG and AMOC changes may mainly reflect their decadal variations[5,10], both the AMOC and SPG are driven by common forcing such as the North Atlantic Oscillation[6], and complex phase lead/lag in the AMOC-SPG coupling when atmosphere-ocean interactions are considered[13,14].

Indeed, aside from recent observations of the transatlantic section at 25°N[4] and RAPID array at 26.5°N in the North Atlantic[15], proxy reconstructions indicate that an AMOC slowing has been present since the middle to late twentieth century[16–18]. The AMOC slowing is expected to continue during the twenty-first century in scenarios like Representative Concentration Pathway 8.5 (RCP8.5)[19] and Shared Socio-economic Pathway 5–8.5 (SSP5–8.5)[20]. Such long-term AMOC decline has the potential to influence the North Atlantic SPG; however, this influence and underlying mechanisms remain largely unknown, as the centurial AMOC change exceeds the aforementioned circulation variability on decadal scales. To tackle this scientific question, here we combine reanalysis data and coupled climate model simulations to investigate the effects and physical mechanisms of AMOC slowdown on global wind-driven circulations, including the North Atlantic SPG, throughout the twenty-first century.

Results

Observed weakening in the AMOC and SPG

We first investigate changes in AMOC strength and barotropic stream function in the North Atlantic using an ensemble of three reanalysis products (Methods). The reanalysis ensemble mean shows an AMOC slowdown from 1980 to 2017 (Fig. 1a) and a declining trend in the North Atlantic SPG during the same period, particularly in the western SPG (Fig. 1b). This finding aligns with previous research[4,5,21], indicating that the AMOC and North Atlantic SPG are weakening in a coherent manner. The eastern North Atlantic SPG, however, is in a strengthening trend (Fig. 1b), which is

Department of Earth and Planetary Sciences, University of California Riverside, Riverside, CA, USA. ✉e-mail: mmimi001@ucr.edu

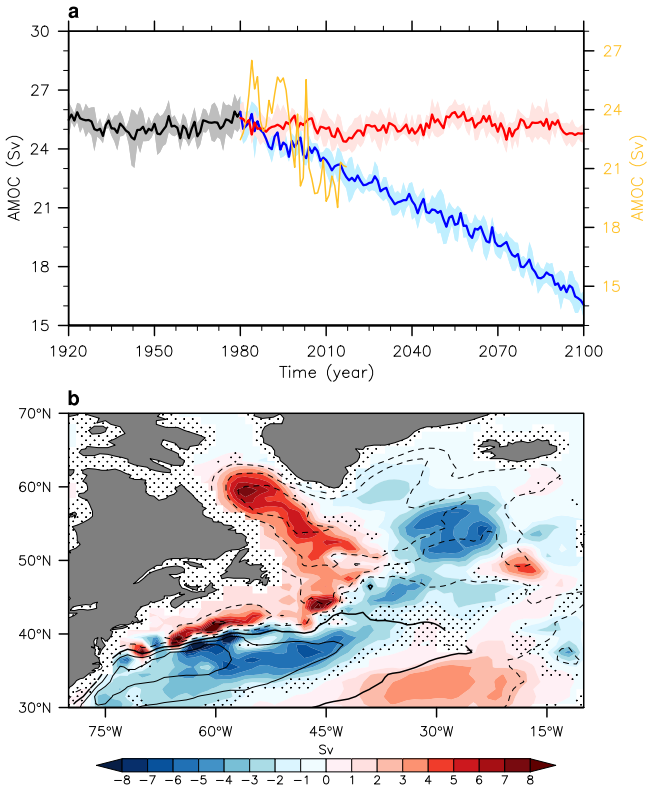

Fig. 1 | Observed AMOC and North Atlantic gyre circulation changes. a AMOC strength (Methods) derived from reanalysis data (the average of GECCO3, ORAS4, and ORAS5, orange), CCSM4 historical plus RCP8.5 simulation (denoted as free-AMOC; prior to 1980, ensemble mean, black; ensemble spread, gray; after 1980, ensemble mean, blue; ensemble spread, light blue) and CCSM4 fixed-AMOC experiment (denoted as fixed-AMOC; ensemble mean, red; ensemble spread, light red) where ensemble spread represents one standard derivation among ensembles. CCSM4 and reanalysis AMOCs reference the left and right areas, respectively. **b** Changes in annual mean barotropic stream function (shading in Sv) between 2000–2017 and 1980–1997 (2000–2017 minus 1980–1997) in the North Atlantic for the average of three reanalysis products. Contours show the annual climatology of barotropic stream function from 1980 to 1997 (solid positive, dashed negative, and zero thickened). The stipples refer to the regions where changes are not significantly different from zero at the 95% confidence level of the Student's *t*-test. The base map is from NCAR Command Language map outline databases.

likely due to the decadal gyre intensification in this region since the mid-2000s[22]. On the other hand, the weakening of the subtropical gyre over the Gulf Stream region, combined with the strengthening of the SPG to the north, forms a dipole pattern, indicative of a northward shift of either the Gulf Steam path or the North Atlantic subtropical gyre[23,24]. Note that these collective changes in the AMOC, North Atlantic gyres, and Gulf Stream path could be heavily influenced by anthropogenic forcing—many of the changes may serve as a direct response to anthropogenic forcing—making it difficult to disentangle the AMOC effect on the North Atlantic SPG and Gulf Stream.

AMOC effects on global wind-driven circulation

To segregate and quantify AMOC effects on the North Atlantic SPG, or more broadly, on global wind-driven circulation within a fully coupled climate system under anthropogenic forcing, we employ a broadly used coupled climate model—Community Climate System Model version 4 (CCSM4; Methods). The ensemble mean of CCSM4 historical plus RCP8.5 simulation (free-AMOC thereafter) describes an AMOC slowdown since the 1980s (Fig. 1a). Over 1980–2017, the trend of AMOC strength (Methods) is -0.69 ± 0.13 Sv per decade (ensemble mean trend ± one standard deviation of the trends among ensembles, 1 Sv = 10^6 m^3 s^{-1}) for the free-AMOC simulation and -1.43 ± 1.11 Sv per decade (reanalysis mean trend ± one standard deviation of the trends among reanalyses) for reanalysis data, which reveals that the simulated AMOC change is within observational uncertainty and, hence, justifies the usage of CCSM4. Based on the free-AMOC simulation, we perform a parallel ensemble simulation with CCSM4 (fixed-AMOC thereafter, Methods) that is driven by the same historical and RCP8.5 forcing agents, with the exception that freshwater is gradually removed from the surface in the deep-water formation areas in the North Atlantic and uniformly redistributed over the rest of the global oceans[25]. This experimental setup contributes to maintaining a constant AMOC strength throughout the twenty-first century (Fig. 1a), even as anthropogenic warming continues. The difference between free- and fixed-AMOC simulations depicts AMOC effects.

We look at and into the ensemble mean results of CCSM4 simulations, with a particular focus on the AMOC effect in the twenty-first century. In the fixed-AMOC simulation, the barotropic stream function exhibits positive and negative anomalies in the North Atlantic SPG and subtropical gyre over 2000–2024 compared to 1961–1980 (Fig. 2c and Supplementary Fig. 1c), suggesting that the SPG weakens, and the subtropical gyre shifts poleward under anthropogenic forcing even in the absence of AMOC slowdown. Compared to the fixed-AMOC simulation, the magnitude of barotropic stream function anomalies in the North Atlantic is larger in the free-AMOC simulation (Fig. 2a and Supplementary Fig. 1a), meaning that the AMOC slowdown significantly weakens the North Atlantic SPG and moves the North Atlantic subtropical gyre poleward (Fig. 2e and Supplementary Fig. 1e). This is because the weakened AMOC creates a dipole-like change in sea level pressure (SLP) in the subpolar North Atlantic—negative SLP anomalies over Greenland and positive SLP anomalies to the south (Fig. 3a)—as a result of a direct linear response to the sea surface temperature (SST) warming minimum in the North Atlantic warming hole[24] combined with an indirect eddy forced response due to the enhanced SST gradient produced by the warming hole[26]. The latter positive SLP anomalies promote anticyclonic surface wind anomalies, which drive anomalous anticyclonic ocean flows, decelerating the North Atlantic SPG (Fig. 3a). Over 2000–2024, the AMOC slows by 0.03 Sv per decade, which yields a weakening of the North Atlantic SPG by -0.05 Sv per decade. We also discover consistent changes in the North Atlantic SPG, SLP, and surface winds over 2076–2100 from the difference between the free- and fixed-AMOC simulations (Fig. 2f, Fig. 3b and Supplementary Fig. 1f), implying that this mechanism is active throughout the twenty-first century.

On the other hand, along with the poleward shift of the North Atlantic subtropical gyre, the weakened AMOC brings about a northward shift in the Gulf Stream path. Here, we use subsurface temperatures near the north wall at a depth of 200 m to indicate the Gulf Stream path[27]. By comparing the free- and fixed-AMOC simulations, we find that the weakened AMOC makes the Gulf Stream shift north, and the shift becomes much larger in the latter period (Supplementary Fig. 2), as consistent with previous findings[12,28].

The AMOC slowdown also manifests fingerprints in upper ocean western boundary currents in the Atlantic in the forms of continuous negative anomalies of barotropic stream function between 40°N and 40°S along the western boundary of the basin (Fig. 2e, f, and Supplementary Fig. 1e, f). Over the period 2000–2024, the weakened AMOC prompts a weaker northward Gulf Stream and Guiana Current, as well as a stronger southward Brazil Current (Supplementary Fig. 3), wherein the latter is important for flow redistribution in the South Atlantic subtropical gyre[29]. The changes in the Guiana and Brazil Currents can be understood from the perspective of oceanic adjustments via oceanic Kelvin and Rossby waves[30]. Oceanic signals in response to freshwater perturbations in the subpolar North Atlantic can propagate to lower latitude North Atlantic and even the South Atlantic via coastal Kelvin waves along the Atlantic's western boundary on interannual timescales[31], and the westward propagation of oceanic Rossby waves emanating from the Atlantic's eastern boundary [32,33] on longer decadal timescales[34]. These fingerprints on the western boundary currents become even more striking toward the end of the twenty-first century (Supplementary Fig. 4). Given that the Gulf Stream has both wind-

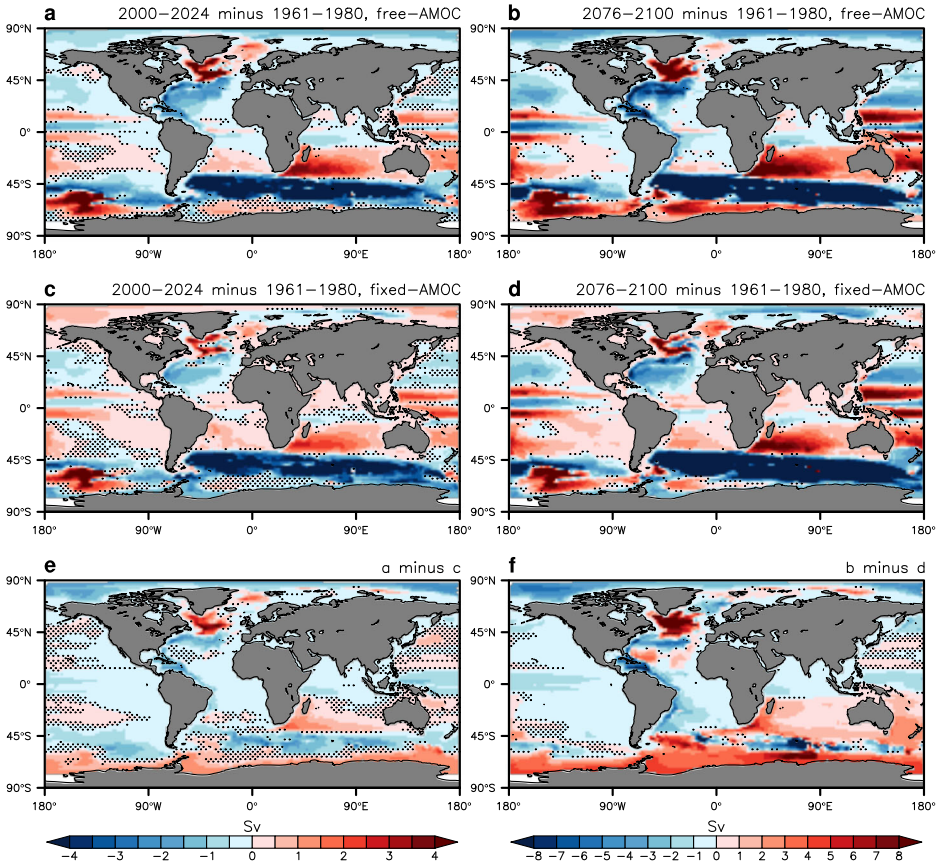

Fig. 2 | Global wind-driven circulation changes and AMOC impacts. a, **c**, **e** Changes in annual mean global barotropic stream function (shading in Sv) for the ensemble means of CCSM4 **a** free- and **c** fixed-AMOC simulations during the period of 2000–2024 relative to 1961−1980, and **e** the difference between the two (a minus c). **b**, **d**, **f** Same as **a**, **c**, **e** but for the period of 2076–2100. The stipples refer to the regions where changes are not significantly different from zero at the 95% confidence level of the Student's *t*-test. The base map is from NCAR Command Language map outline databases.

driven and thermohaline components, our free- and fixed-AMOC simulations delineate that changes in the wind-driven part are much smaller than those in the thermohaline part in a warming climate (Supplementary Figs. 3a–c and 4a–c). While a surface warming effect[35] may play a role in the AMOC-induced acceleration of the Brazil Current. The Guiana Current, on the other hand, weakens under anthropogenic forcing if the AMOC keeps steady, but strengthens when the AMOC slows (Supplementary Figs. 3d–f and 4d–f), which demonstrates the central role of the AMOC in controlling future changes in this ocean current.

The AMOC affects wind-driven circulation not only in the Atlantic, but also in the Southern Ocean (Fig. 3 and Fig. 4). Between 2000 and 2024, the AMOC slowdown causes a SLP change in a pattern similar to the positive Southern Annular Mode (Fig. 3c). Corresponding to the SLP change, Southern Hemisphere surface westerly winds display a poleward displacement (Fig. 3c), whose zonal mean exhibits positive and negative anomalies to the south and north of 55°S (Fig. 4c). Such surface winds drive a poleward shifted Deacon cell (Fig. 4f), which is partially mediated by eddy-induced meridional overturning circulation (MOC, Fig. 4i). As a result, the residual MOC response generally follows the change in the Deacon Cell, producing a poleward-shifted residual MOC in the Southern Ocean (Fig. 4l). Via altering Southern Hemisphere surface westerly winds, the AMOC slowdown also generates a dipole-like change in the barotropic stream function in the Southern Ocean, with negative anomalies typically around 45–60°S and positive anomalies to the south, indicative of a poleward shift of the Antarctic Circumpolar Current (Fig. 2e).

In particular, the AMOC slowdown remotely alters Southern Hemisphere winds and Southern Ocean circulation[36,37] through the following mechanism. During 2000–2024, the weakened AMOC reduces northward oceanic heat transport, giving rise to tropospheric warming in the Southern Hemisphere (Fig. 5a). The most pronounced warming occurs around 55°S, with poleward temperature gradient increasing south of 55°S but decreasing toward the north. Such temperature gradient changes intensify and weaken the Southern Hemisphere jets on their poleward and equatorward flanks, respectively (Fig. 5b), prompting poleward displacements of Southern Hemisphere westerly winds and Ferrell cell (Fig. 5c). Relative to 1961–1980, poleward shifts of Southern Hemisphere westerly winds, the Deacon cell, Southern Ocean residual MOC and Antarctic Circumpolar Current are also present over the period of 2076–2100 (Fig. 3d, Supplementary Fig. 5), albeit the dipole-like changes in westerly winds and associated changes in the Deacon cell and residual MOC appear smaller than those in 2000–2024, whereupon the aforementioned mechanism is in effect throughout the twenty-first century (Supplementary Fig. 6). It merits attention that, besides the atmospheric teleconnection, a weakened AMOC could have a conspicuous effect on ocean circulation changes in the southern Indian Ocean and Antarctic Circumpolar Current via oceanic bridges[38]. The weakened Atlantic overturning causes positive sea level anomalies to propagate into the Cape of Good Hope and the southern Indian Ocean as Kelvin waves via oceanic waveguides, modulating the Antarctic Circumpolar Current through wave–current interactions[38].

Evidence from multi-model large ensembles

In addition to our full-physics free- and fixed-AMOC experiments, independent evidence from other sources also supports the important role of AMOC slowdown in wind-driven circulation. Here, we leverage the large ensemble simulations with CESM1 under historical and RCP8.5 scenarios, CESM2 under historical and SSP3–7.0 scenarios, and ACCESS1-ESM1.5 and MPI-ESM1.2-MR under historical and SSP5-8.5 scenarios. The underlying rationale is that, even under the same external anthropogenic forcing, individual ensemble members simulate varying degrees of AMOC decline throughout the twenty-first century due to internal variability. A comparison of these members thus helps to reveal the AMOC effect. This approach is in line with previous analysis using inter-model difference in the coupled model intercomparison project[39]—verified by EC-Earth3 fixed-AMOC simulations[40]—pertaining to AMOC impacts under abruptly quadrupled CO_2 scenario. In particular, for each model, we calculate the Atlantic barotropic stream function and AMOC strength anomalies for all

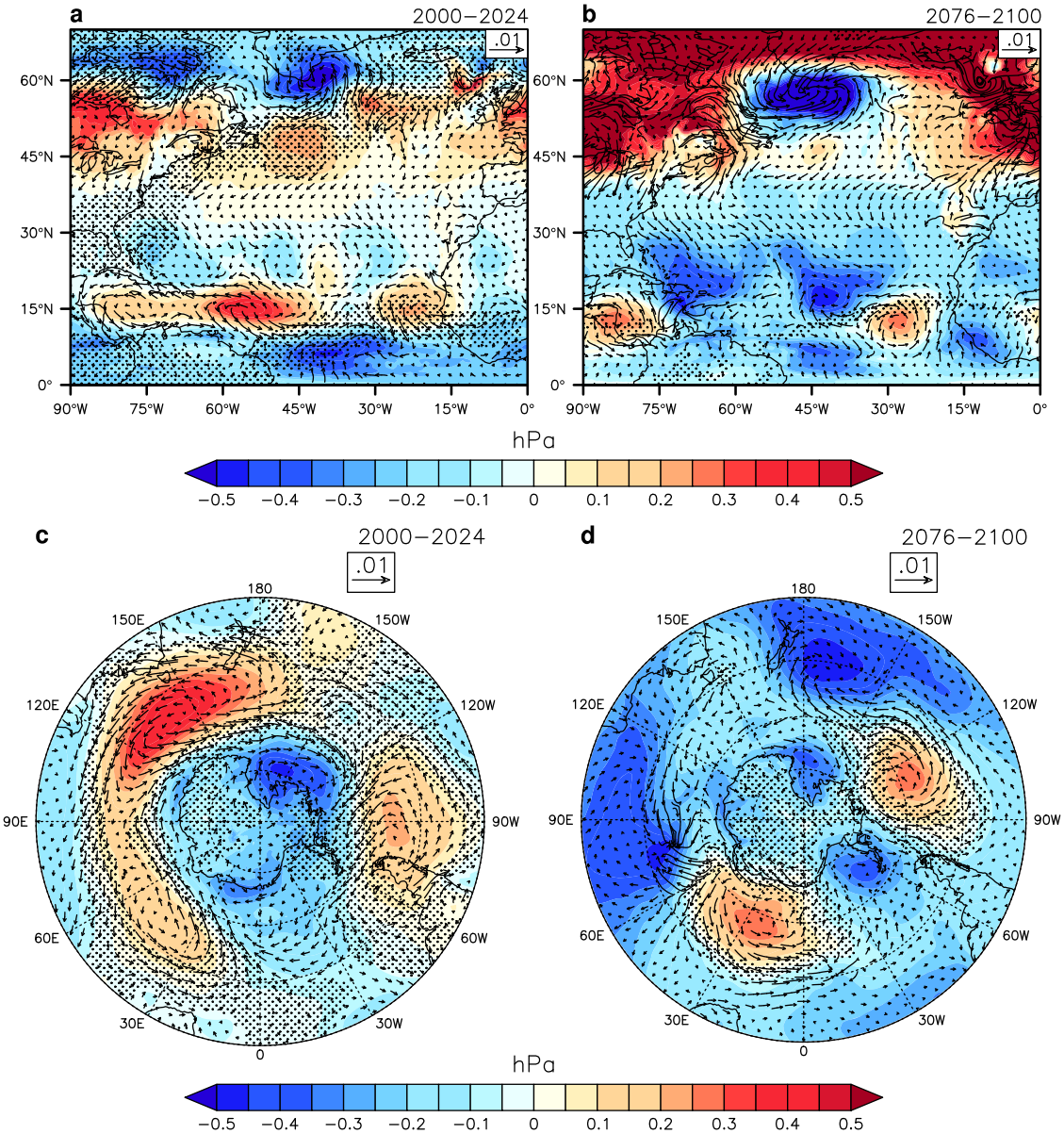

Fig. 3 | AMOC effects on sea level pressure and surface wind stress. a, **b** Differences of annual mean sea level pressure (shading in hPa) and wind stress (vectors in N/m^2) between the ensemble means of CCSM4 free- and fixed-AMOC simulations (free minus fixed) over the North Atlantic during **a** 2000–2024 and **b** 2076–2100 relative to 1961–1980. **c**, **d** As in **a**, **b** but for the Southern Ocean. The stipples refer to the regions where differences are not significantly different from zero at the 95% confidence level of the Student's *t*-test. The base map is from NCAR Command Language map outline databases.

members over the periods of 2000–2024 and 2076–2100 relative to 1961–1980, respectively, and exploit inter-member differences to estimate the response of Atlantic barotropic stream function to 1-Sv AMOC decline during the two periods via linear regression ("Methods"). We find that an AMOC slowdown is associated with a decelerated North Atlantic SPG, along with poleward shifts of the North Atlantic subtropical gyre and Gulf Stream path, and aforementioned fingerprints in the western boundary currents in the North Atlantic for all four models during the periods of 2000–2024 (Fig. 6) and 2076–2100 (Supplementary Fig. 7). This result evinces that the AMOC effect derived from CCSM4 experiments is robust across a broad range of models and global warming scenarios.

Conclusions

In this study, we use fully coupled climate model simulations to elucidate the effect of AMOC slowdown on wind-driven circulation over the twenty-first century. We find that the weakened AMOC causes positive SLP and anticyclonic surface wind anomalies over the subpolar North Atlantic, which slows the North Atlantic SPG. The decelerated Atlantic overturning also has fingerprints on upper ocean western boundary currents in the Atlantic, such as a weaker northward Gulf Stream and Guiana Current and a stronger southward Brazil Current. Beyond the Atlantic, the weakened AMOC promotes a poleward displacement of Southern Hemisphere surface westerly winds by altering meridional gradients of atmospheric temperature, which renders poleward shifts of the Deacon cell, residual MOC in the Southern Ocean, and Antarctic Circumpolar Current. Our findings highlight the significance of the atmospheric response to AMOC slowdown in modulating wind-driven circulation on a global scale.

Methods

Reanalysis data

We employ three ocean reanalysis products to derive AMOC strength and barotropic stream function, namely the ocean synthesis contributed by the German Estimating the Circulation and Climate of the Ocean version 3 (GECCO3), Ocean Reanalysis System 4 (ORAS4) and 5 (ORAS5) from the

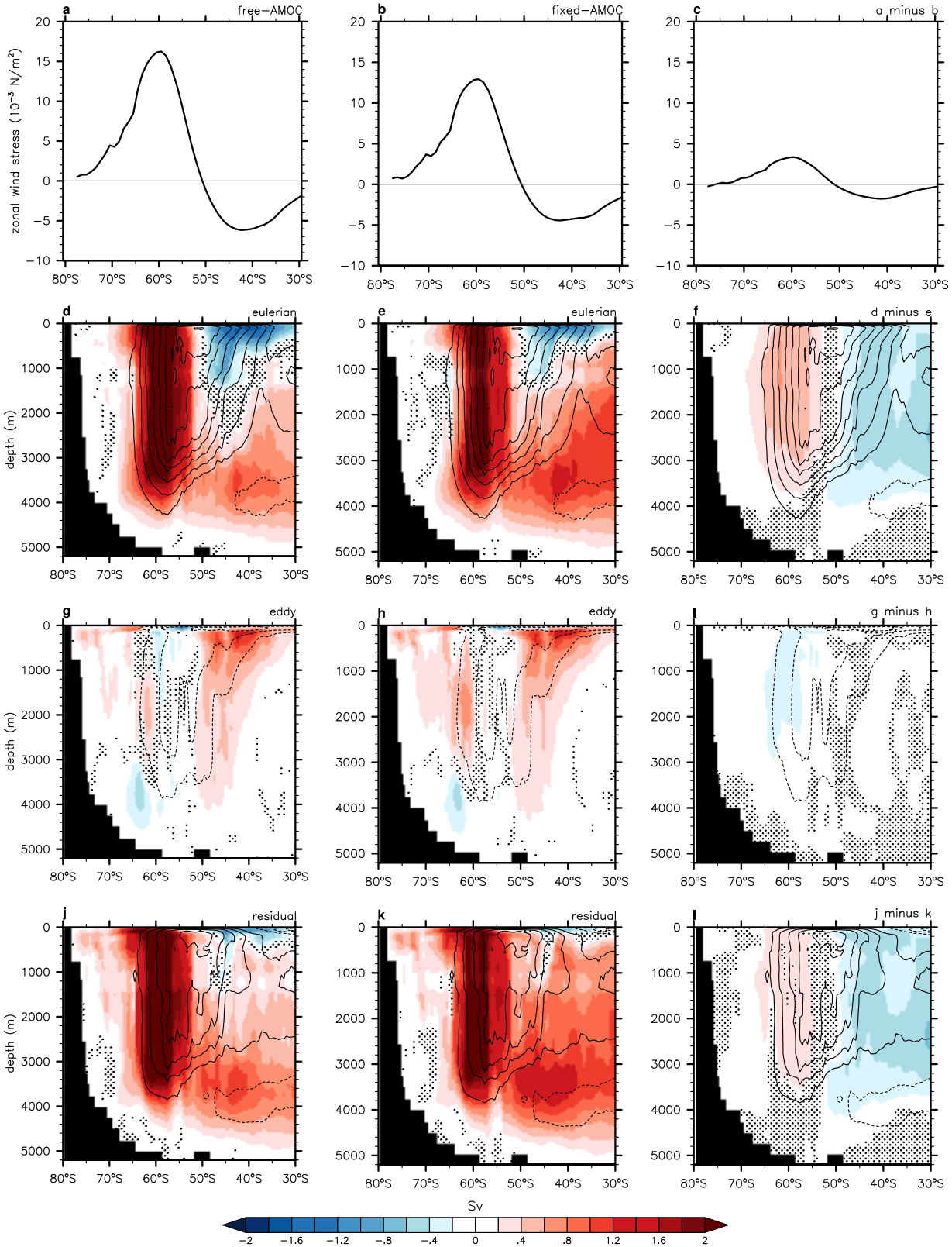

Fig. 4 | AMOC effects on Southern Ocean surface winds and MOCs over 2000–2024. a–c Changes in annual and zonal mean zonal wind stress to the south of 30°S during 2000–2024 relative to 1961–1980 for the ensemble means of CCSM4 **a** free- and **b** fixed-AMOC simulations, and **c** the difference between the two (free minus fixed). **d–f** Same as **a–c** but for annual mean Eulerian-mean MOC in the Southern Ocean (shading in Sv). **g–i** Same as **d–f** but for eddy-induced MOC. **j–l** Same as **d–f** but for residual MOC. In **d–l**, the overlapping black contour lines (in Sv, with an interval of 5 Sv, solid positive, dashed negative, and zero omitted) in each panel denote the annual and ensemble mean during 1961–1980, and the stipples refer to the regions where changes are not significantly different from zero at the 95% confidence level of the Student's *t*-test.

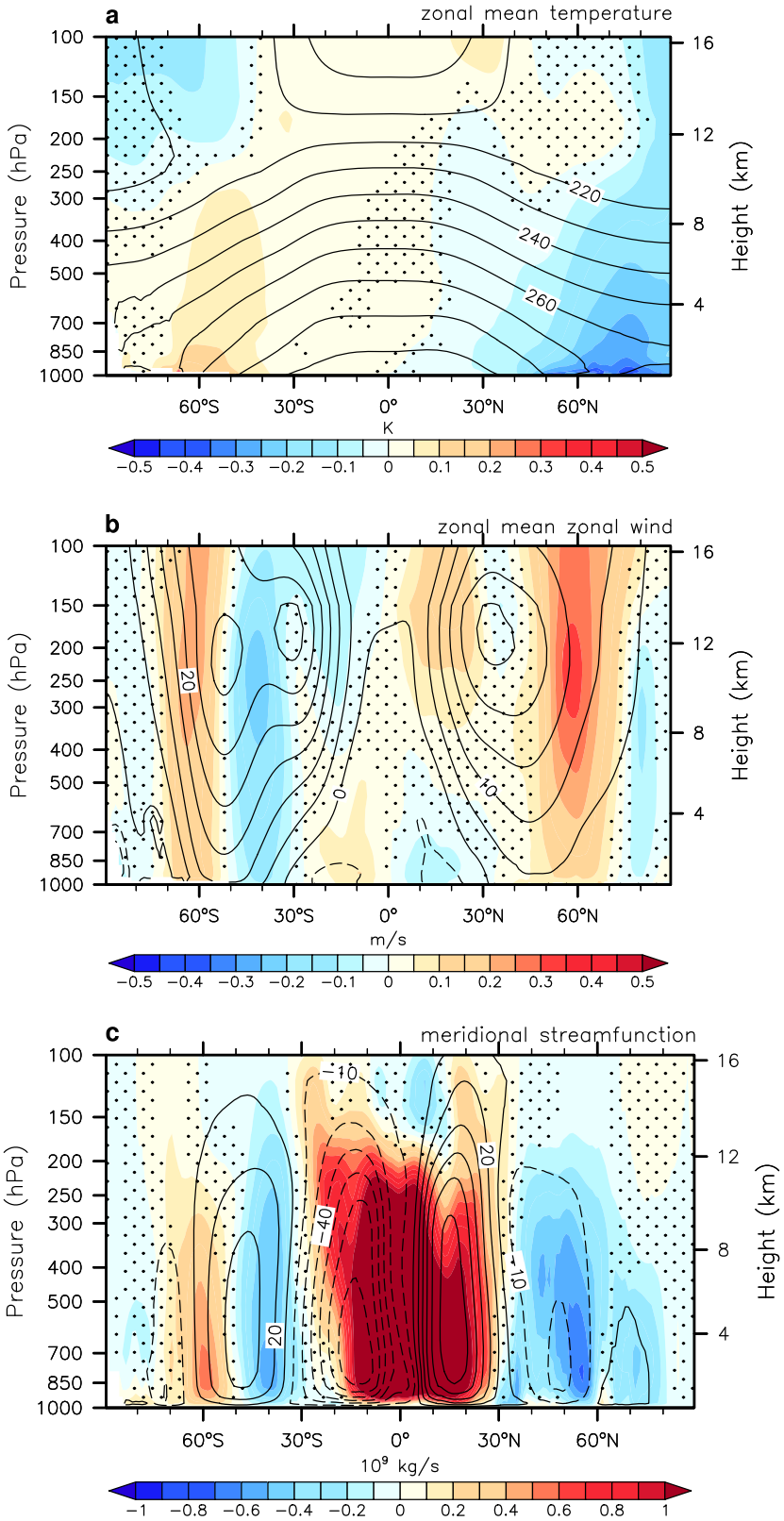

Fig. 5 | AMOC effects on atmospheric temperature and circulation over 2000–2024. Differences of annual and zonal mean **a** atmospheric temperature (shading in K) and **b** zonal winds (shading in m/s), and **c** annual mean meridional stream function (shading in 10^9 kg/s) during 2000–2024 relative to 1961–1980. The overlapping black contour lines in each panel denote the annual mean during 1961–1980. The stipples refer to the regions where differences are not significantly different from zero at the 95% confidence level of the Student's *t*-test.

European Centre for Medium-Range Weather Forecasts. The monthly GECCO3 data[41] have a nominal horizontal resolution of 0.4° × 0.4° and 40 vertical levels, spanning from 1948 to 2018. The monthly ORAS4 data[42] have a horizontal resolution of approximately 1° × 1° and 42 vertical levels, spanning from 1958 to 2017. The monthly ORAS5 data[43] starts from 1979 and has a horizontal resolution of approximately 0.25° × 0.25° and 75 vertical levels. For each reanalysis product, we calculate the Atlantic meridional overturning stream function (ψ) at the depth z from the meridional velocity (v) as,

$$\psi(y,z) = \int_{z}^{0}\int_{x_w}^{x_e} v(x,y,z')\,dxdz' \quad (1)$$

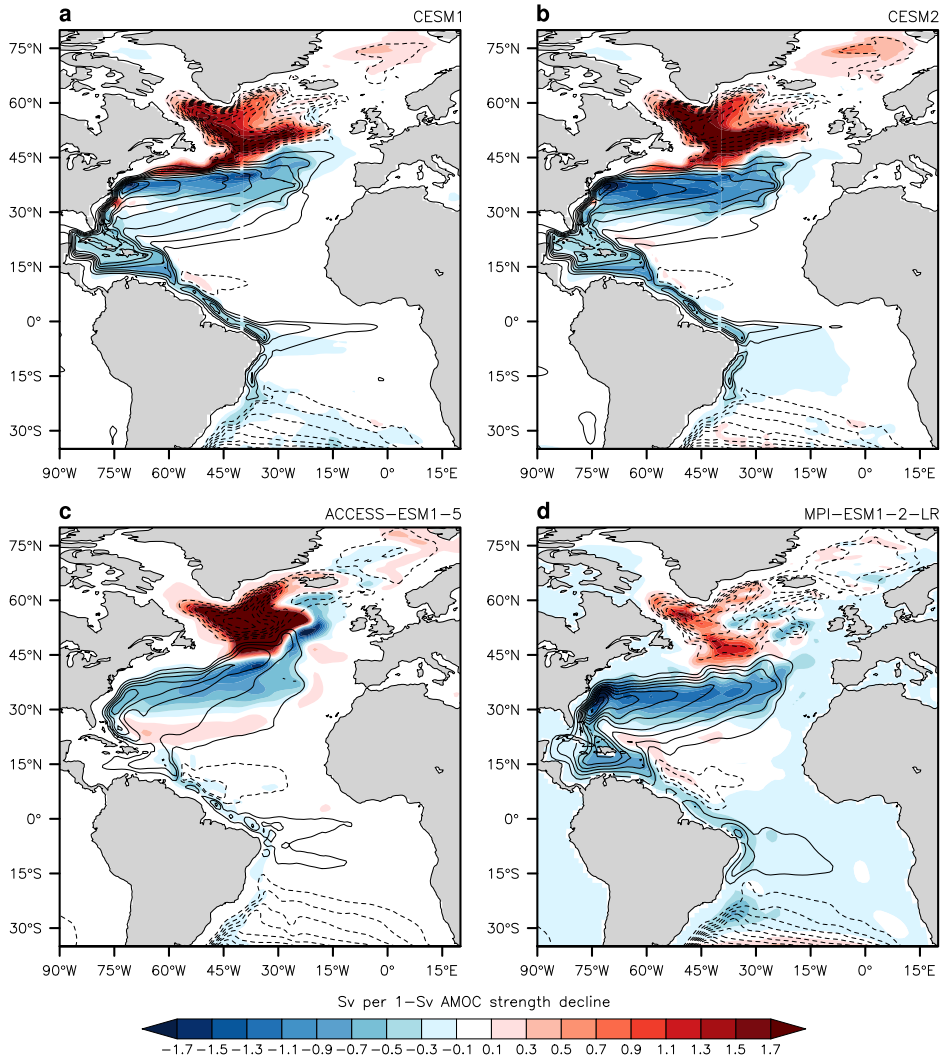

Fig. 6 | Intermodel comparison for the period of 2000–2024. Barotropic stream function response to 1-Sv AMOC slowdown (shading in Sv) via linear regression based on inter-member differences of changes in annual mean barotropic stream function and AMOC strength over 2000–2024 relative to 1961–1980 for **a** CESM1, **b** CESM2, **c** ACCESS-ESM1-5, and **d** MPI-ESM1-2-LR large ensemble simulations (Methods). Contours (in Sv, with an interval of 5 Sv, solid positive, dashed negative, and zero omitted) indicate the annual mean barotropic stream function averaged over the 1961–1980 period. The base map is from NCAR Command Language map outline databases.

where x, y, and z' represent the zonal, meridional, and vertical depth coordinates, and x_w and x_e denote the western and eastern boundaries of the Atlantic Ocean. AMOC strength is defined as the maximum annual mean meridional stream-function below 500 m in the North Atlantic. We examine the changes in AMOC strength during the period from 1980 to 2017, when all the reanalysis products have data available.

CCSM4 free- and fixed-AMOC experiments

We use CCSM4, which combines the Community Atmosphere Model version 4, Community Land Model version 4, Community Ice CodE version 4, and Parallel Ocean Program version 2, featuring an atmospheric resolution of approximately one degree and an ocean resolution nominally set at one degree[44]. We investigate five ensemble members from CCSM4 historical plus RCP8.5 (referred to as free-AMOC) simulation. The CCSM4 free-AMOC simulation exhibits a deceleration of the AMOC since the 1980s in the historical plus RCP8.5 scenario, which is consistent with findings from reanalysis data (Fig. 1a) and many other climate models[19]. We also perform a five-ensemble sensitivity (referred to as fixed-AMOC) experiment in which freshwater is extracted from the North Atlantic deep-water formation region to sustain the AMOC strength[24]. This experiment started in 1980 and shares the same historical (prior to 2005) and RCP8.5 (after 2005) forcing agents with the free-AMOC simulation. However, it entails gradually removing freshwater from the region north of 50°N in the North Atlantic, Labrador, Greenland, Iceland, and Norwegian Seas, and redistributing freshwater uniformly across the global oceans as outlined by refs. 25,45–48. The local modification of surface freshwater flux in the North Atlantic, Labrador, Greenland, Iceland, and Norwegian Seas has few direct effects on salinity in other ocean basins, such as the Southern Ocean, on the timescales of interest.

Multi-model large ensemble simulations

We exploit large ensemble simulations conducted with four different climate models that provide barotropic stream function outputs. They are CESM1 with 40 members under historical and RCP8.5 scenarios spanning from 1920 to 2100[49], CESM2 with 50 members under historical and SSP3–7.0 scenarios spanning from 1850 to 2100[50], ACCESS-ESM1.5 with 50 members under historical and SSP5–8.5 scenarios spanning from 1850 to 2100[51], and MPI-ESM1.2-MR with 50 members under historical and SSP5–8.5 scenarios spanning from 1850 to 2100[52]. For each model, we first calculate Atlantic barotropic stream function and AMOC strength anomalies for all members over the periods of 2000–2024 and 2076–2100 relative to 1961–1980, respectively. For both periods, we calculate the linear regression coefficient on each grid between barotropic stream function anomaly and AMOC strength anomaly of ensemble members and multiply (−1) Sv to illustrate the response of barotropic stream function to 1-Sv AMOC decline.

Significance tests

We use a Student's t-test to determine the statistical significance of linear trend. We calculate the p-value to determine whether the linear trend differs significantly from a zero trend. We also test the difference between CCSM4 free- and fixed-AMOC simulations for significance at the 95% confidence

level using the Student's *t*-test to illustrate when and where AMOC impacts are significant relative to internal climate variability.

Reporting summary

Further information on research design is available in the Nature Portfolio Reporting Summary linked to this article.

Data availability

Data from CESM1 and CESM2 large ensemble simulations, and CCSM4 historical and RCP8.5 simulations are available at https://www.earthsystemgrid.org. Data from ACCESS-ESM1.5 and MPI-ESM1.2-MR large ensemble simulations are available at https://aims2.llnl.gov/search/cmip6/. The fixed-AMOC experiment was conducted with a modified source code of CCSM4 based on ref. 24, and the source code of CCSM4 is available at https://www.cesm.ucar.edu/models/ccsm4.0/.

Code availability

The source code of CCSM4 is available at https://www.cesm.ucar.edu/models/ccsm4.0/. Figures are generated via the NCAR Command Language (NCL, Version 6.5.0) [Software]. (2018). Boulder, Colorado: UCAR/NCAR/CISL/TDD (https://doi.org/10.5065/D6WD3XH5).

Received: 25 July 2024; Accepted: 13 November 2024;
Published online: 21 November 2024

References

1. MacMynowski, D. G. & Tziperman, E. Two-way feedback interaction between the thermohaline and wind-driven circulations. *J. Phys. Oceanogr.* **36**, 914–929 (2006).
2. Timmermann, A. & Goosse, H. Is the wind stress forcing essential for the meridional overturning circulation? *Geophys. Res. Lett.* **31**, L20705 (2004).
3. Yang, H., Wang, K., Dai, H., Wang, Y. & Li, Q. Wind effect on the Atlantic meridional overturning circulation via sea ice and vertical diffusion. *Clim. Dyn.* **46**, 3387–3403 (2016).
4. Bryden, H. L., Longworth, H. R. & Cunningham, S. A. Slowing of the Atlantic meridional overturning circulation at 25°N. *Nature* **438**, 655–657 (2005).
5. Häkkinen, S. & Rhines, P. B. Decline of subpolar North Atlantic circulation during the 1990s. *Science* **304**, 555–559 (2004).
6. Böning, C. W., Scheinert, M., Dengg, J., Biastoch, A. & Funk, A. Decadal variability of subpolar gyre transport and its reverberation in the North Atlantic overturning. *Geophys. Res. Lett.* **33**, L21S01 (2006).
7. De Coetlogon, G. et al. Gulf Stream variability in five oceanic general circulation models. *J. Phys. Oceanogr.* **36**, 2119–2135 (2006).
8. Larson, S. M., Buckley, M. W. & Clement, A. C. Extracting the buoyancy-driven Atlantic meridional overturning circulation. *J. Clim.* **33**, 4697–4714 (2020).
9. Ma, X. et al. Evolving AMOC multidecadal variability under different CO_2 forcings. *Clim. Dyn.* **57**, 593–610 (2021).
10. Zhang, R. Coherent surface-subsurface fingerprint of the Atlantic meridional overturning circulation. *Geophys. Res. Lett.* **35**, L20705 (2008).
11. Zhang, R. et al. A review of the role of the Atlantic meridional overturning circulation in Atlantic multidecadal variability and associated climate impacts. *Rev. Geophys.* **57**, 316–375 (2019).
12. Joyce, T. M. & Zhang, R. On the path of the Gulf Stream and the Atlantic meridional overturning circulation. *J. Clim.* **23**, 3146–3154 (2010).
13. Wen, N., Frankignoul, C. & Gastineau, G. Active AMOC–NAO coupling in the IPSL-CM5A-MR climate model. *Clim. Dyn.* **47**, 2105–2119 (2016).
14. Sun, J., Latif, M. & Park, W. Subpolar gyre–AMOC–atmosphere interactions on multidecadal timescales in a version of the Kiel climate model. *J. Clim.* **34**, 6583–6602 (2021).
15. Smeed, D. A. et al. The North Atlantic Ocean is in a state of reduced overturning. *Geophys. Res. Lett.* **45**, 1527–1533 (2018).
16. Rahmstorf, S. et al. Exceptional twentieth-century slowdown in Atlantic ocean overturning circulation. *Nat. Clim. Change* **5**, 475–480 (2015).
17. Thornalley, D. J. et al. Anomalously weak Labrador sea convection and Atlantic overturning during the past 150 years. *Nature* **556**, 227–230 (2018).
18. Caesar, L., McCarthy, G., Thornalley, D., Cahill, N. & Rahmstorf, S. Current Atlantic meridional overturning circulation weakest in last millennium. *Nat. Geosci.* **14**, 118–120 (2021).
19. Weaver, A. J. et al. Stability of the Atlantic meridional overturning circulation: a model intercomparison. *Geophys. Res. Lett.* **39**, L20709 (2012).
20. Weijer, W., Cheng, W., Garuba, O. A., Hu, A. & Nadiga, B. CMIP6 models predict significant 21st century decline of the Atlantic meridional overturning circulation. *Geophys. Res. Lett.* **47**, e2019GL086075 (2020).
21. Tietsche, S. et al. The importance of North Atlantic ocean transports for seasonal forecasts. *Clim. Dyn.* **55**, 1995–2011 (2020).
22. Chafik, L., Nilsen, J. E. Ø., Dangendorf, S., Reverdin, G. & Frederikse, T. North Atlantic ocean circulation and decadal sea level change during the altimetry era. *Sci. Rep.* **9**, 1041 (2019).
23. Yang, H. et al. Intensification and poleward shift of subtropical western boundary currents in a warming climate. *J. Geophys. Res.* **121**, 4928–4945 (2016).
24. Yang, H. et al. Poleward shift of the major ocean gyres detected in a warming climate. *Geophys. Res. Lett.* **47**, e2019GL085868 (2020).
25. Liu, W., Fedorov, A. V., Xie, S.-P. & Hu, S. Climate impacts of a weakened Atlantic meridional overturning circulation in a warming climate. *Sci. Adv.* **6**, eaaz4876 (2020).
26. Gervais, M., Shaman, J. & Kushnir, Y. Impacts of the North Atlantic warming hole in future climate projections: mean atmospheric circulation and the North Atlantic jet. *J. Clim.* **32**, 2673–2689 (2019).
27. Frankignoul, C., de Coëtlogon, G., Joyce, T. M. & Dong, S. Gulf Stream variability and ocean–atmosphere interactions. *J. Phys. Oceanogr.* **31**, 3516–3529 (2001).
28. Caesar, L., Rahmstorf, S., Robinson, A., Feulner, G. & Saba, V. Observed fingerprint of a weakening Atlantic ocean overturning circulation. *Nature* **556**, 191–196 (2018).
29. Marcello, F., Tonelli, M., Ferrero, B. & Wainer, I. Projected Atlantic overturning slowdown is to be compensated by a strengthened South Atlantic subtropical gyre. *Commun. Earth Environ.* **4**, 92 (2023).
30. Kawase, M. Establishment of deep ocean circulation driven by deep-water production. *J. Phys. Oceanogr.* **17**, 2294–2317 (1987).
31. Zhang, R. Latitudinal dependence of Atlantic meridional overturning circulation (AMOC) variations. *Geophys. Res. Lett.* **37**, L16703 (2010).
32. Huang, R. X., Cane, M. A., Naik, N. & Goodman, P. Global adjustment of the thermocline in response to deepwater formation. *Geophys. Res. Lett.* **27**, 759–762 (2000).
33. Johnson, H. L. & Marshall, D. P. A theory for the surface Atlantic response to thermohaline variability. *J. Phys. Oceanogr.* **32**, 1121–1132 (2002).
34. Cessi, P., Bryan, K. & Zhang, R. Global seiching of thermocline waters between the Atlantic and the Indian–Pacific ocean basins. *Geophys. Res. Lett.* **31**, L04302 (2004).
35. Peng, Q. et al. Surface warming-induced global acceleration of upper ocean currents. *Sci. Adv.* **8**, eabj8394 (2022).
36. Chen, C., Liu, W. & Wang, G. Understanding the uncertainty in the 21st century dynamic sea level projections: The role of the AMOC. *Geophys. Res. Lett.* **46**, 210–217 (2019).
37. Zhang, L., Delworth, T. L. & Zeng, F. The impact of multidecadal Atlantic meridional overturning circulation variations on the Southern ocean. *Clim. Dyn.* **48**, 2065–2085 (2017).

38. Peng, Q. et al. Indonesian throughflow slowdown under global warming: remote AMOC effect versus regional surface forcing. *J. Clim.* **36**, 1301–1318 (2023).
39. Bellomo, K., Angeloni, M., Corti, S. & von Hardenberg, J. Future climate change shaped by inter-model differences in Atlantic meridional overturning circulation response. *Nat. Commun.* **12**, 3659 (2021).
40. Bellomo, K. & Mehling, O. Impacts and state-dependence of AMOC weakening in a warming climate. *Geophys. Res. Lett.* **51**, e2023GL107624 (2024).
41. Köhl, A. Evaluating the GECCO3 1948–2018 ocean synthesis–a configuration for initializing the MPI-ESM climate model. *Q. J. R. Meteorol. Soc.* **146**, 2250–2273 (2020).
42. Balmaseda, M. A., Trenberth, K. E. & Källén, E. Distinctive climate signals in reanalysis of global ocean heat content. *Geophys. Res. Lett.* **40**, 1754–1759 (2013).
43. Zuo, H., Balmaseda, M. A., Tietsche, S., Mogensen, K. & Mayer, M. The ECMWF operational ensemble reanalysis–analysis system for ocean and sea ice: a description of the system and assessment. *Ocean Sci.* **15**, 779–808 (2019).
44. Gent, P. R. et al. The community climate system model version 4. *J. Clim.* **24**, 4973–4991 (2011).
45. Liu, W., Duarte Cavalcante Pinto, D., Fedorov, A. & Zhu, J. The impacts of a weakened Atlantic meridional overturning circulation on ENSO in a warmer climate. *Geophys. Res. Lett.* **50**, e2023GL103025 (2023).
46. Ren, X. & Liu, W. The role of a weakened Atlantic meridional overturning circulation in modulating marine heatwaves in a warming climate. *Geophys. Res. Lett.* **48**, e2021GL095941 (2021).
47. Lee, Y.-C. & Liu, W. The weakened Atlantic meridional overturning circulation diminishes recent Arctic sea ice loss. *Geophys. Res. Lett.* **50**, e2023GL105929 (2023).
48. Lee, Y.-C., Liu, W., Fedorov, A. V., Feldl, N. & Taylor, P. C. Impacts of Atlantic meridional overturning circulation weakening on Arctic amplification. *Proc. Natl Acad. Sci. USA* **121**, e2402322121 (2024).
49. Kay, J. E. et al. The community earth system model (CESM) large ensemble project: A community resource for studying climate change in the presence of internal climate variability. *Bull. Am. Meteorol. Soc.* **96**, 1333–1349 (2015).
50. Rodgers, K. B. et al. Ubiquity of human-induced changes in climate variability. *Earth Syst. Dyn.* **12**, 1393–1411 (2021).
51. Ziehn, T. et al. The Australian earth system model: access-esm1.5. *J. South. Hemisph. Earth Syst. Sci.* **70**, 193–214 (2020).
52. Gutjahr, O. et al. Max Planck institute earth system model (MPI-ESM1. 2) for the high- resolution model intercomparison project (HighResMIP). *Geosci. Model Dev.* **12**, 3241–3281 (2019).

Acknowledgements

This study has been supported by U.S. National Science Foundation (OCE-2123422, AGS-2053121, and AGS-2237743).

Author contributions

M.S.M. performed the analysis and wrote the original draft of the paper. W.L. conceived the study and conducted CCSM4 fixed-AMOC experiment. Both authors contributed to interpreting the results and made improvements to the paper.

Competing interests

The authors declare no competing interests.

Additional information

Supplementary information The online version contains supplementary material available at https://doi.org/10.1038/s43247-024-01907-5.

Correspondence and requests for materials should be addressed to Mohima Sultana Mimi.

Peer review information *Communications Earth & Environment* thanks Kay McMonigal and the other, anonymous, reviewer(s) for their contribution to the peer review of this work. Primary Handling Editor: Alireza Bahadori. A peer review file is available